Korean J. Chem. Eng., 40(1), 37-45 (2023)
DOI: 10.1007/s11814-022-1273-2

pISSN: 0256-1115
eISSN: 1975-7220

Exploring advanced process equipment visualization as a step towards digital twins development in the chemical industry: A CFD-DNN approach

Dela Quarme Gbadago*, Jiyoung Moon*,, and Sungwon Hwang*,**,†**

*Department of Chemistry and Chemical Engineering, Education and Research Center for Smart Energy and Materials, Inha University, Incheon 22212, Korea
**Department of Smart Digital Engineering, Inha University, Incheon 22212, Korea
(*Received 1 June 2022 • Revised 5 August 2022 • Accepted 24 August 2022*)

Abstract−Several studies involving the implementation of artificial neural network (ANN) technology for process design, monitoring, and control are under active research. This new technology has shown great potential in advancing chemical processes through the development of digital twins and smart factories. In joining this race, the current study explores the capability of physics-based modeling (CFD) and artificial neural networks for advanced process data visualization. Here, 20 CFD simulations of a multi-tubular reactor equipped with a Zn-Fe-Cr catalyst for synthesizing butadiene were executed. The simulation result was extracted as 3-D data with XYZ coordinates and imported into a python-based DNN model for training and cross-validation. An accuracy of 99.2% was obtained from the ANN surrogate model. The trained model was used to predict 3D data in terms of the process temperature, concentration, etc. The 3D data was then imported into a Paraview® VTK for detailed virtualization. Cross-sectional, longitudinal, and radial distribution of the various process variables, such as concentration profiles and pressure contour, were effectively visualized. A graphic user interface was further developed using Python for real-time visualization of the equipment. This implementation is analogous to the digital twin and is employable for online system optimization, high accuracy, low computational cost, and seamlessly integrable 3D real-time visualization system design for efficient, quick, and easy plant decision-making.

Keywords: Digital Twins, CFD, Artificial Intelligence, Deep Neural Networks, Optimization, Chemical Industry

INTRODUCTION

The fourth industrial revolution--the integration of the internet of things [1], information and communication technology [2], and cyber-physical systems [3]--is paving the way for the development of smart factories [4] and advanced manufacturing [5]. A common name among industry and academia is the digital twin [1,2, 4-14], a digital duplicate of a physical system. The capability of the new technology provides a new paradigm shift for advanced process integration, visualization, and control for the effective management of process systems. In this regard, several research from industrial players [9,15] has undertaken to explore potential and efficient ways of deploying digital twins [1,2,4-14,16]. While progress is being made in the various reports, one major aspect of the digital twin that poses many challenges is the seamless integration and visualization of process equipment using simulation tools towards advanced intepretability and projection of engineering processes. ANSYS Fluent and ThingWorx [8] collaborated to provide a CFD platform for integrating physical systems with digital twins for improved process visualization and decision making. However, considering the computational cost of CFD simulation, it is almost impossible to seamlessly integrate them with physical processes in real-time. In line with these developments, academics have also shown great interest in this new research area. For example, a recent study by [17] proposed a framework to combine artificial intelligence with mathematical modeling, machine learning, and 2D visualization tools for process data prediction. This new technology is expected to make the plant operation easier and more efficient. Kim et al. [18] also developed an LSTM-RNN model, which uses sensor data generated by CFD simulation to predict suspected leakage locations in real-time. As a result, the leakage position can be quickly identified, and an effective initial response can be performed. Despite these efforts, limited research is available on this significant aspect of engineering. The detailed visualization of process equipment performance in real-time analogous to the digital twin is not available in the open literature, limiting digital twins to computationally expensive models that are impossible to integrate seamlessly with real processes. In addition, critical process equipment, such as reactors, has not been fully digitized to provide detailed online visualization of their performance and risk assessment for good decision making due to the limitations of sensors and other process monitoring devices.

Hence in this study, a hybrid-based 3D chemical process visualization strategy is provided as an alternative to model-based digital twins for seamless integration into a digital twin platform. The strategy is based on a computational fluid dynamics model employed for 3D data generation, which is used for training a highly efficient and accurate deep neural network surrogate model for predicting three-dimensional (3D) data for advanced visualization of the desired

†To whom correspondence should be addressed.
E-mail: sungwon.hwang@inha.ac.kr

process variables. The 3D data are imported into VTK software (Paraview) for rendering. The detailed behavior of the process equipment based on changes in the plant operation can be visualized in real-time using this strategy. Our goal is to leverage rigorous mathematical modeling with an AI-integrated system for real-time process equipment monitoring and visualization. Furthermore, a graphic user interface was developed to display the 3D results in real-time, analogous to the digital twin. The method is also useful for online optimization of process variables, efficient manipulation of control variables, and predictive maintenance. Furthermore, the VTK back code also generates a glTF image, a high-definition 3D image format with embedded information that otherwise is unavailable in png and jpeg format images. These generated 3D images are also imported into Unity3D to create a mixed reality environment that can be deployed into Hololens2 for complete immersive visualization and interaction with the process performance.

The rest of the text is organized as follows: Section 2 discusses the mathematical theories and models developed in this study. Then, in section 3, the results are presented and subsequently discussed. Finally, the conclusion is presented in section 4.

MATHEMATICAL MODELLING

1. Physics-based Modeling

This section elaborates the mathematical modeling techniques and conservation equations that were employed in executing the CFD simulations. It also includes the development of surrogate models and genetic algorithms.

1-1. Mass Continuity

The mass continuity equation is calculated according to Eq. (1):

$$\frac{\partial \rho}{\partial t} + \nabla \cdot (\rho \vec{u}) = \dot{R} \tag{1}$$

where ρ, u, and R are the density, velocity, and mass source terms, respectively.

1-2. Momentum Conservation

The momentum transport equation for the pressure-velocity coupling is written as follows:

$$\frac{\partial}{\partial t}(\rho \vec{u}) + \nabla(\rho \vec{u}\vec{u}) = -\nabla p + \rho \vec{g} + \nabla(\tau + \tau_t) + \dot{R}\vec{u} + S \tag{2}$$

where μ, g, R, p, S are the dynamic viscosity, gravity, reaction source term, pressure, porous resistance in that order.

1-3. Energy Conservation

The general energy balance equation for the reactor system is written as:

$$\frac{\partial}{\partial t}(\rho h) + \nabla \cdot (\rho \vec{u} h) + \frac{\partial}{\partial t}(\rho k) + \nabla \cdot (\rho \vec{u} k) - \frac{\partial p}{\partial t} = \rho \vec{u}\vec{g} + \nabla \cdot (\alpha_{eff} \nabla h) + \dot{Q}_{rxn} \tag{3}$$

where h is the specific enthalpy, k is the turbulent kinetic energy, Q_{rxn} is the heat source due to chemical reactions, α_{eff} is the effective thermal diffusivity (contribution of laminar and turbulent diffusivities).

1-4. Species Transport Equation

The mass concentrations of the individual gas species are computed according to:

$$\varepsilon_p \frac{\partial}{\partial t}(\rho Y_i) + \varepsilon_p \nabla \cdot (\rho \vec{u} Y_i) - \varepsilon_p \nabla \cdot (\rho D_i \nabla Y_i) = (1 - \varepsilon_p)\rho_{cat} \dot{R}_i \tag{4}$$

where, Y, D, R, ρ_{cat}, are the mass fraction of species, the diffusivity, the species reaction source term, and the catalyst density, respectively. The species conservation equation is calculated such that the total mass fraction is unity Eq. (5).

$$\sum_{i=1}^{n} Y_i = 1 \tag{5}$$

The reaction mechanism of Sterret et al. [19] on the conversion of butene to butadiene via the oxidative dehydrogenations reactions was used in this study (Eqs. (6)-(11)). Here, heat evolution from the three reactions is expected with a consequent increase in reaction zone temperature.

$$C_4H_8 + 0.5O_2 \xrightarrow{r_1} C_4H_6 + H_2O \quad \Delta H_r = -128.1 \text{ kJ/mol} \tag{6}$$

$$C_4H_8 + 6O_2 \xrightarrow{r_2} 4CO_2 + 4H_2O \quad \Delta H_r = -2{,}552.6 \text{ kJ/mol} \tag{7}$$

$$C_4H_6 + 5.5O_2 \xrightarrow{r_2} 4CO_2 + 3H_2O \quad \Delta H_r = -2{,}394.5 \text{ kJ/mol} \tag{8}$$

$$r_1 = \frac{A_1 e^{-E_1/RT} P_B^n P_{O2}}{(1 + K_{O2}P_{O2})(1 + K_B P_B + K_{BD} P_{BD})} \tag{9}$$

$$r_2 = \frac{A_2 e^{-E_2/RT} P_{O2}(P_B - 3P_{BD})}{(1 + K_{O2}P_{O2})(K_B P_B + K_{BD} P_{BD})} \tag{10}$$

$$r_3 = \frac{A_3 e^{-E_3/RT} P_{O2} P_{BD}}{(1 + K'_{O2}P_{O2})(P_B + P_{BD})} \tag{11}$$

Detailed reaction parameters are available in our previous research [13].

2 CFD Simulation for Data Generation

The mass continuity, momentum equation, energy transport energy, and the species conservation equations presented in Section 2 were hardcoded into an OpenFOAM v2006 package for computing the CFD simulation. The CFD model was validated against the experimental results of Sterrett et al [19]. The time step was automatically adjusted such that the total courant number was 1 to maintain the numerical stability, accuracy, and convergence of the model. The timestep ranged from 10^{-6} to 10^{-4}. The input param-

Table 1. CFD simulation input parameters

	Variable	Value	Unit
Operating conditions	Gas flowrate	0.007	kg/s
	Coolant velocity	1	m/s
	porosity	0.39	-
	Temperature	variable	K
	Pressure	101325	Pa
Mole fractions	C_4H_8	0.05	-
	H_2O	0.047	-
	O_2	0.717	-
	N_2	0.186	-
Catalyst	Density	4806	kg/m^3
	Thermal cond.	0.2514	W/mk

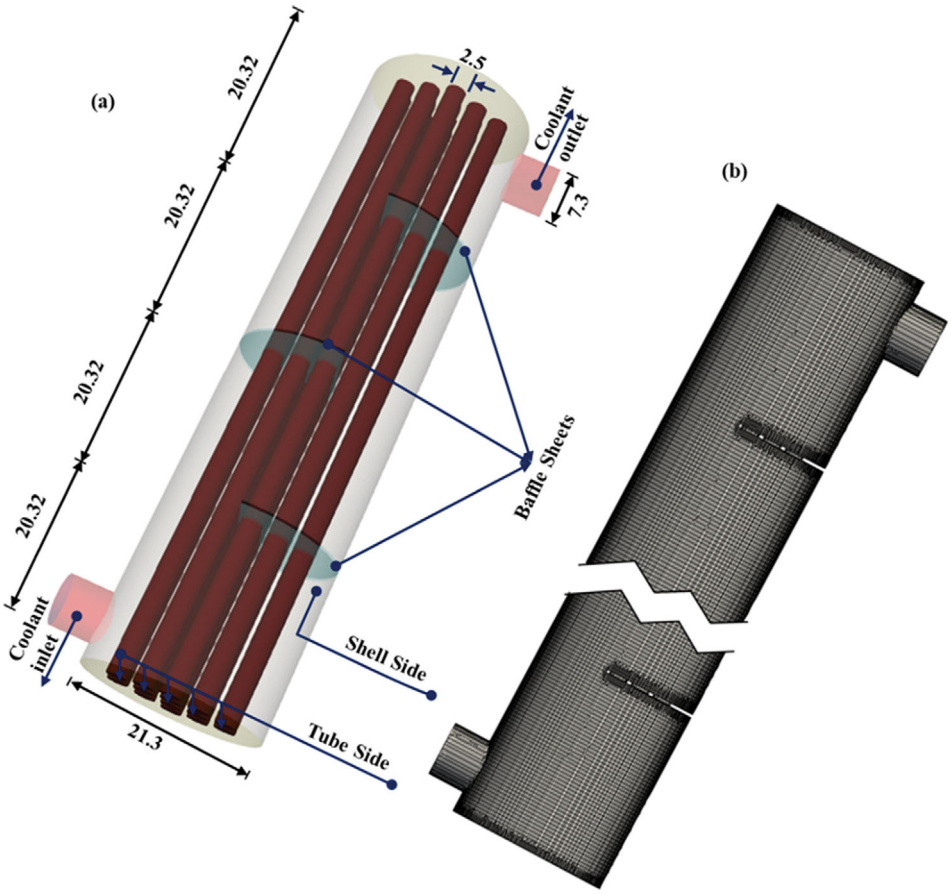

Fig. 1. Multi-tubular reactor for the case study (a) geometry, (b) mesh.

eters according to Table 1 were fed into the CFD package for geometry design and subsequent simulation. The data for the simulation are presented in Table 1. Twenty (20) CFD simulations were carried out by varying the input temperature between 630 K and 730 K to generate data for training the DNN model. The geometry and mesh employed here are also presented in Fig. 1.

3. DNN Model Development

A two-layer feed forward-backward propagation multilayer perceptron referred to as the DNN model with 79 and 85 neurons was developed to train the CFD data. The model was coded in Python language using TensorFlow APIs such as Keras, NumPy, Keras, and an early stop to eliminate overfitting. Adam optimizer was used to reduce the gradient of the weights and biases with Selu and LeakyRelu activation functions used to transform the inputs from one layer to another. Four thousand (4000) epochs and a learning rate of 0.1 were also employed. Both the mean absolute error and the mean squared error were used as loss functions in training to ensure the accuracy of the neural network. The data were divided into training, validation, and testing sets in the ratio: 80 : 10 : 10, respectively. The hyperparameters mentioned above were extracted from a genetic algorithm integrated into the neural to automatically search suitable parameters, such as the number of neurons, epochs, activation functions, optimizer, loss functions, and learning rate. A decaying rate was used to eliminate the possibility of the network being stuck at local minima. Early stopping was also employed to prevent the overfitting of the model. The genetic algorithm was developed with ten generations, 100 populations, and a mutation probability of 20%. The best population is selected based on its fitness score, which is the accuracy of the neural network.

4. Process Variable Prediction and Visualization

A dynamic generator was developed to periodically change the process input temperature to mimic a real-life dynamic industrial process where the input variables change with time due to disturbances or noise. The new temperature is then fed to the developed neural network for predicting the various contours. Next, a 3D datatype is predicted and passed to a batch code developed for rendering the generated data into 3D images using Paraview VTK software. The generated images are in two forms, a png file format image, and a glTF 3D image. The png image was imported into a GUI that we developed for real-time visualization. The glTF was employed in a unity3D environment and subsequent deployment in hololens2 for a mixed reality experience that provides higher immersion, interaction, and visualization of the equipment performance results. This allows for a more interactive visualization of the equipment performance, which may not be possible with a normal 3D image viewer or renderer. This is also useful for training and discussion purposes in understanding the complex behavior of the process variables under consideration. For instance, vortices formed around baffles in multi-tubular reactors can be easily visualized and well understood using the interactive toolkit. Fig. 2 shows the

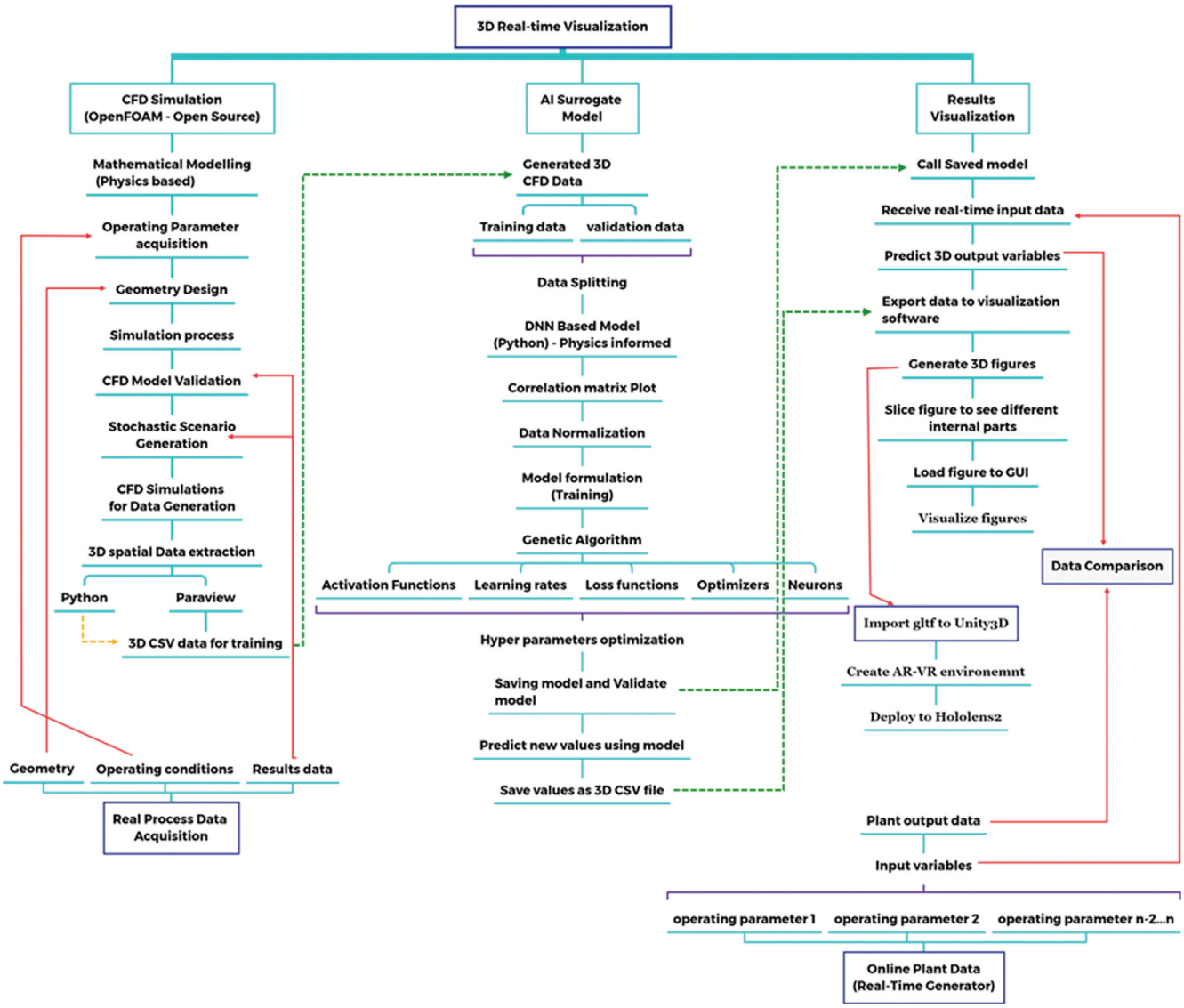

Fig. 2. Overall process methodology for the proposed AI-based real-time process visualization system (digital twin).

Table 2. Data format for the DNN training model

SN	X	Y	Z	T	C_4H_6	C_4H_8	CO_2	O_2
1	−8.49E-07	0.036	0.00980	729.9	0.0206	0.1879	0.00038	0.1129
2	−1.05E-02	0.047	0.00981	731.71	0.0209	0.1875	0.00039	0.1128
.	.	.	.	.	.	.	.	.
1,404,898	−0.0026	0.045	1.0000	599.52	0.1777	0.0247	0.03355	0.3952
1,404,899	0.0026	0.050	1.0000	599.15	0.1775	0.0249	0.03348	0.3951

detailed flow of the implementation of the methodology.

RESULTS AND DISCUSSION

The principal goal of this research is to provide a direction for developing digital twins or real-time advanced process equipment visualization through physics-based mathematical models and artificial neural networks. To achieve this, the methodologies described in chapter 2 were executed. Following successful validation of our physics-based mathematical model (CFD simulation, section 3.1), 20 data sets were generated by varying the input temperature of the butadiene synthesis process. The format of the data is presented in Table 2. Each data set consisted of 1,404,899 data points with X, Y, Z coordinates and the respective process variables of interest. These data sets were used to train neural networks capable of predicting the tube and shell side temperature distributions, butadiene, butene,

oxygen, and carbon dioxide concentrations with response to changes in the input temperature in real-time. The prediction model was developed with Python and integrated with a Paraview batch code that was able to import the predicted data and render it into two types the 3D images, namely, png, and glTF. The developed graphic user interface was then employed to display these png results on a

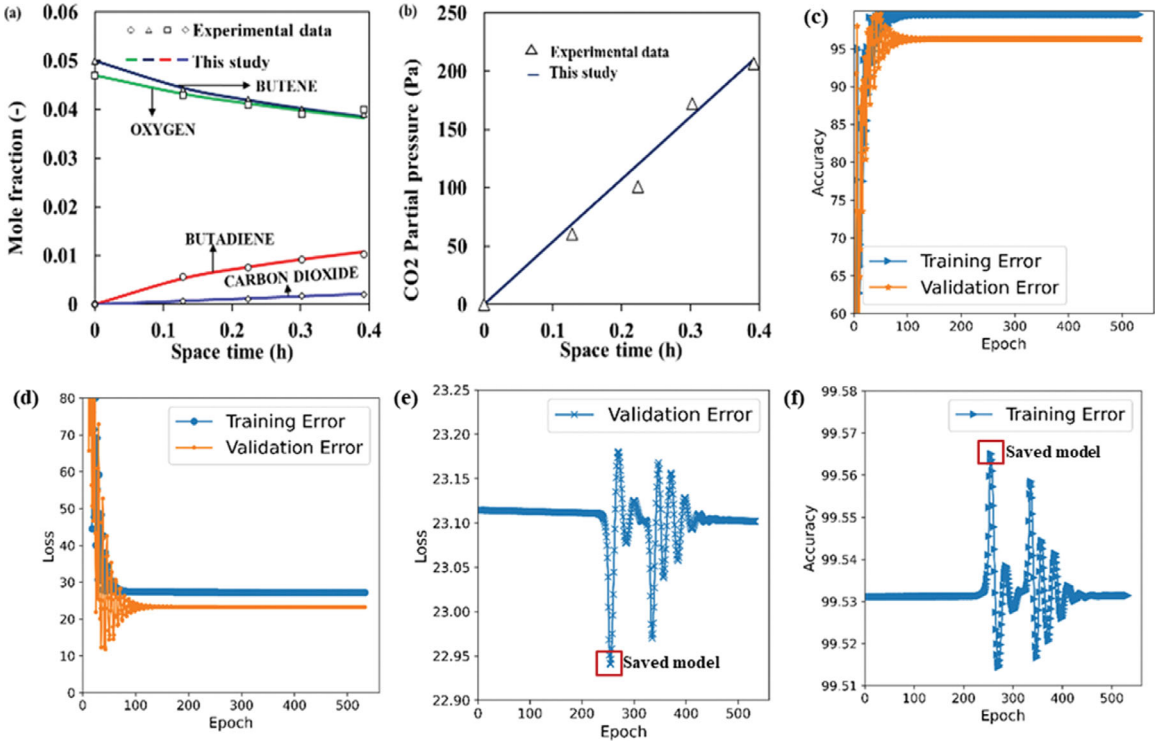

Fig. 3. Model validation results (a) CFD mole fraction of species, (b) CFD CO_2 partial pressure (c) DNN model's accuracy, (d) DNN model's loss, (e) DNN validation loss (model saving instance), (f) DNN training accuracy (model saving instance).

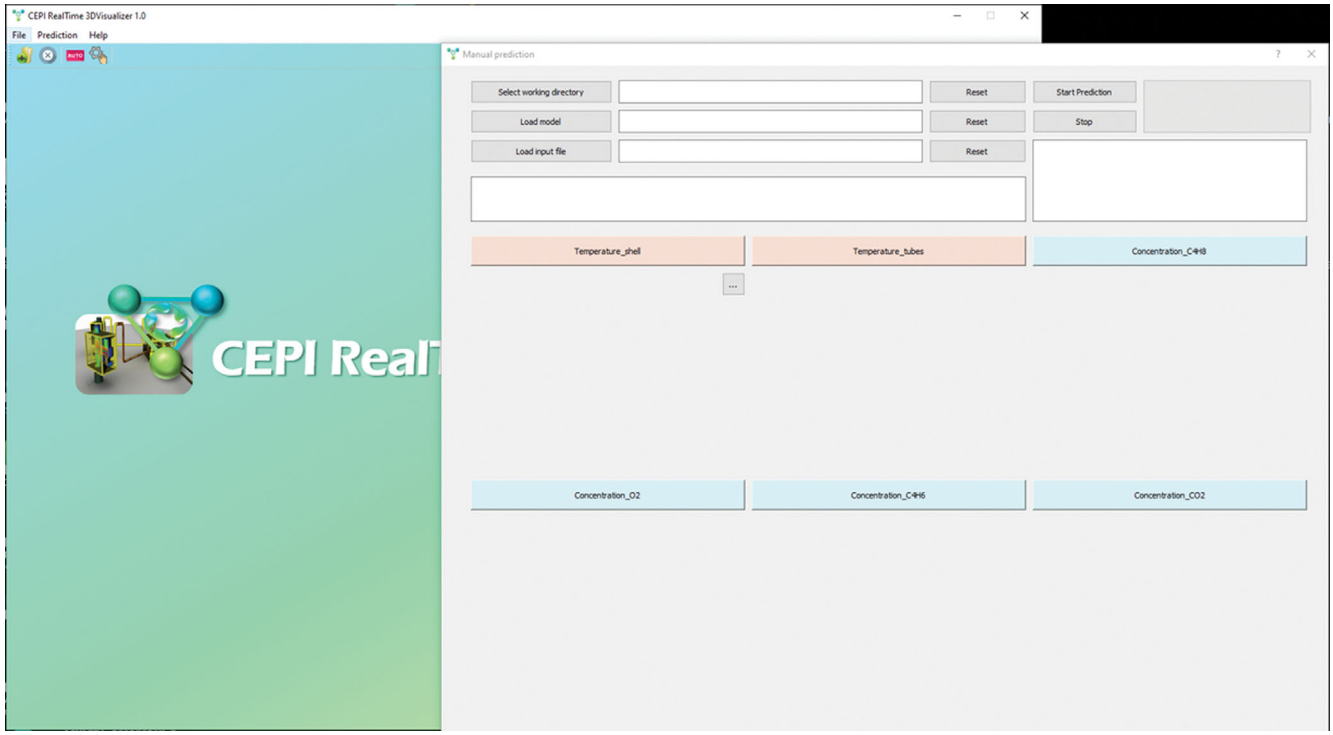

Fig. 4. Developed real-time visualizer interface.

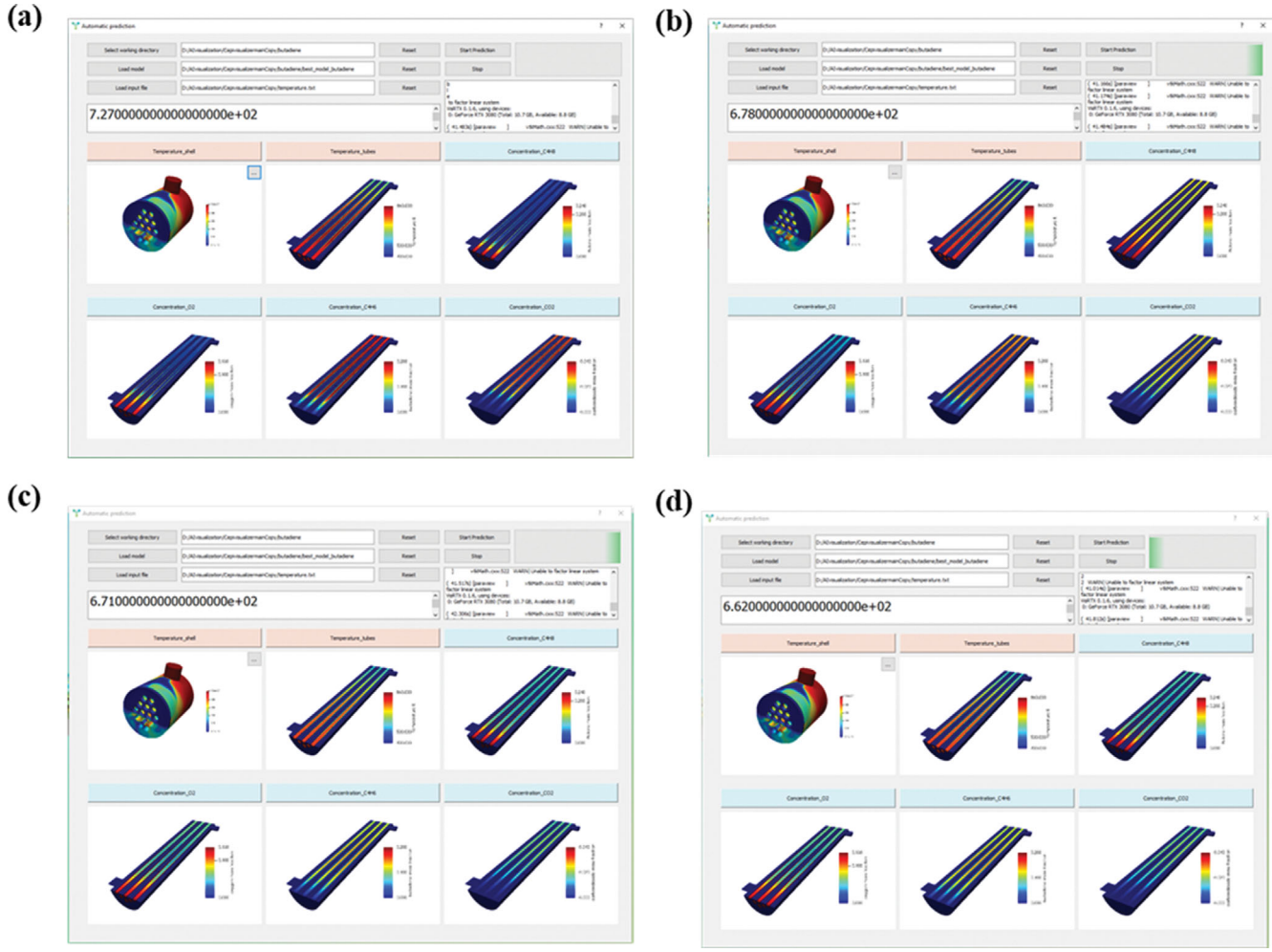

Fig. 5. Displayed real-time prediction results at different process input temperatures (a) 727 K, (b) 678 K, (c) 671 K, and (d) 662 K.

computer screen as soon as the model generates them.

1. CFD and DNN Model Validation

The developed CFD model was validated against the butadiene, butene, CO_2, and O_2 mole fractions and the CO_2 partial pressure against space time, as shown in Fig. 3(a) and (b). Here, an accuracy of 98.2% was obtained from the comparative study, confirming the robustness of the developed CFD model. Furthermore, the DNN model prediction result was compared with the CFD results (Fig. 3(c) and 3(d)) with only a 0.44% error (99.56%) accuracy for the training data and 98.32% for the validation data. The points training instances where the best models were saved are shown in Fig. 3(e) (minimum loss) and Fig. 3(f) (maximum accuracy). These indicate that both the CFD and DNN models were robustly developed for accurate simulations and predictions.

2. Process Equipment Data Visualization

Fig. 4 shows the interface of the visualizer. The current implementation accepts both automatic and manual capabilities. In the former, the generator representing the dynamic input of a real process is used to provide the input variables that the neural network uses to predict the next state of the process in terms of the concentration of O_2, butadiene (C_4H_6), butene (C_4H_8), and CO_2, and the temperature of the reactor. In the manual visualizer option, the plant operator can input the expected input temperature from which the expected process outputs are shown on the panel (computer screen) for visualization. This is particularly helpful in cases where the plant operating conditions need to be changed. The engineers can visualize *a posteriori* the performance of the process in line with the new process conditions. Specifically, in gas turbines where different feed compositions are often encountered, this system can resolve process uncertainties and enhance efficiency, easy decision-making, and overall profitability.

Fig. 5 shows the process outputs of the case study employed here for different input temperatures. The developed framework has well captured the differences in concentration and temperature profiles. From the figure, at input temperatures of 727 K (Fig. 5(a)), 678 K (Fig. 5(b)), 671 K (Fig. 5(c)), and 662 K (Fig. 5(d)), the real-time visualizer displays the different profiles within 30 s of the input. The developed model well predicted all likely conditions of the process. For example, at a very low temperature (643 K, Fig. 6), the visualizer displayed process outputs that correspond precisely to this input condition, indicating the robustness of the model to capture sudden fluctuations in the process feed conditions. Here, very low concentrations of butadiene and CO_2 were generated with high reactant concentrations depicting a low reaction rate.

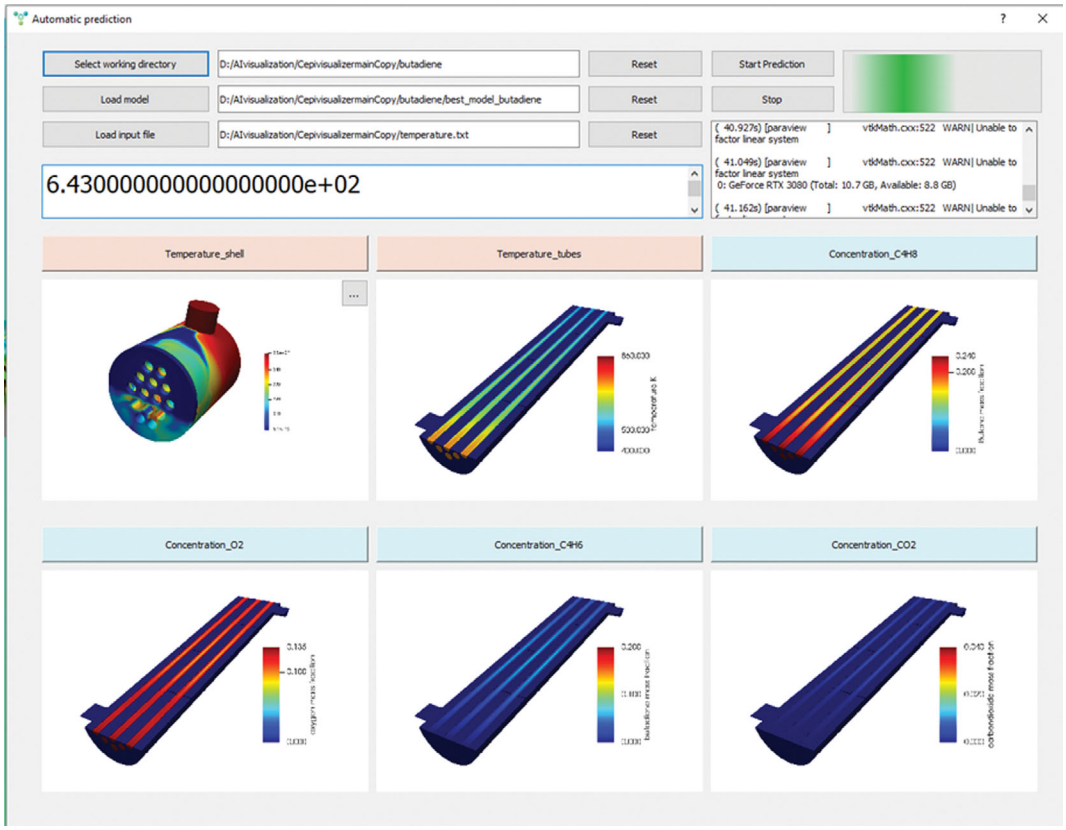

Fig. 6. Reactor performance output at a low input temperature.

Fig. 7. Graphics language transmission format (glTF) images generated by the developed DNN platform for use in virtual reality environments.

As mentioned, the framework generates both png and glTF 3D images. The png images are displayed on the panel (graphic interface). On the other hand, glTF images (Fig. 7) are employed in a mixed reality visualization due to their high-quality data structures to further enhance viewing and analysis of the equipment's performance.

The glTF images were imported into Unity-3D®, preprocessed with a glTF plugin, rendered with a mixed reality tool kit (MRTK), then finally deployed into the HoloLens2 using Microsoft Visual Studio®. Fig. 9 shows a graphical representation of some results obtained from the Hololens2 mixed reality visualization. Fig. 8 shows the buttons plate for selecting the type of process output to visualize, including an animation of the flow field. Fig. 9(a)-9(d) shows some of the selected process variables subsequently displayed for complete immersion and interaction. All objects in the scene can be interacted with by moving, zooming, rotating, and using voice commands to show or hide them. Thus, both the physical and virtual environments can be observed, as demonstrated in the figures. This experience brings the entire process to life, allowing engineers and decision-makers to have a much more detailed understanding of the phenomena that characterize the process. The scenes can also be projected onto other displays, such as laser projectors for group visualization.

Finally, a summarized representation of the entire process implemented here is presented in Fig. 10. From the figure, the developed framework realized significant savings in time and computational cost from 1,768 hours spent on CFD simulations to 6 hours in developing the DNN model to only 30 s for the online prediction and visualization. This suggests that the developed system can seamlessly be integrated with real-life industrial processes to monitor, control, and optimize online systems at low computational burden. In addition, the predicted data is also readily available for plant decision-making and preventive maintenance forecasts. Thus, this proposed strategy is applicable to several critical engineering pro-

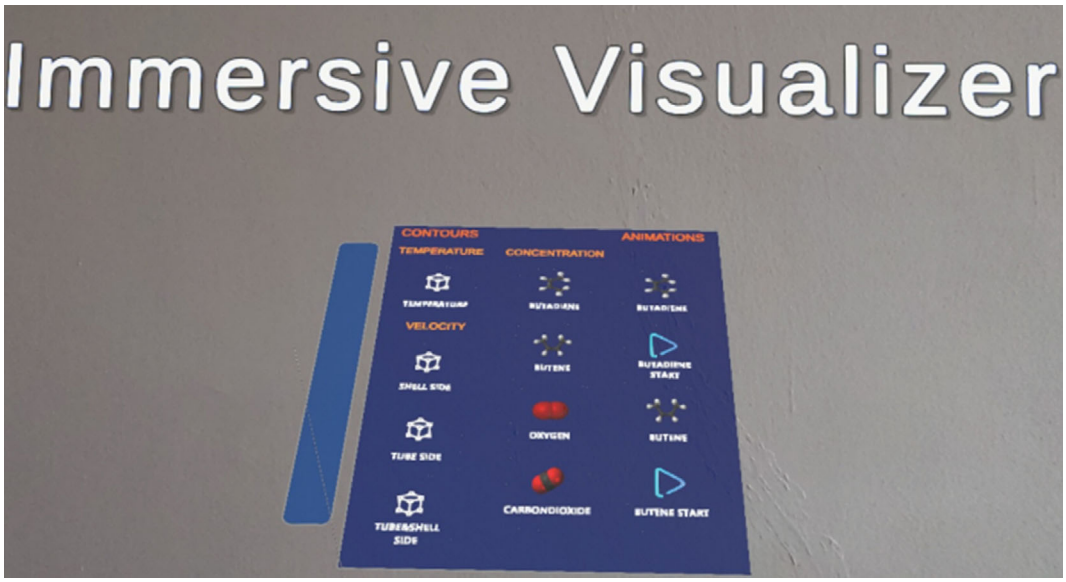

Fig. 8. Title and buttons plate for interacting with the mixed reality environment.

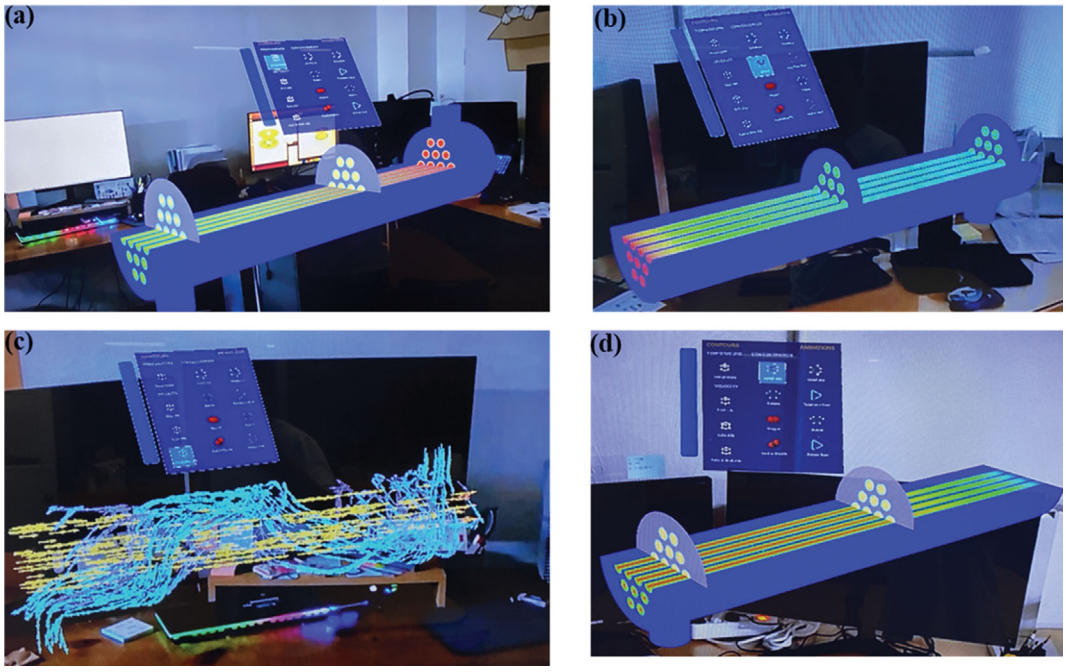

Fig. 9. Virtual reality environment for immersive data visualization experience.

cesses to achieve high fidelity process management and efficiency to overcome the drawbacks of current visualization and digital twin approaches implemented in both academia and industry.

CONCLUSION

We have demonstrated the employability of an integrated physics-based mathematical model (CFD simulation), deep neural networks, Paraview VTK package, and a developed graphic user interface for real-time process equipment performance visualization as a step towards the development of digital twins for critical engineering processes. We employed the CFD model to generate 20 simulation cases by varying the input temperature. Data from these simulations were extracted as 3D data with Cartesian coordinates along with their respective process variables, such as concentrations and temperature. The data were used to train a deep neural network affixed with a genetic algorithm to search the appropriate hyperparameters of the models. The developed deep neural network was integrated with a prediction model to receive a dynamic temperature input value and then predict the required process outputs according to this input condition. The predicted data were then imported seamlessly into a written Paraview batch code for ren-

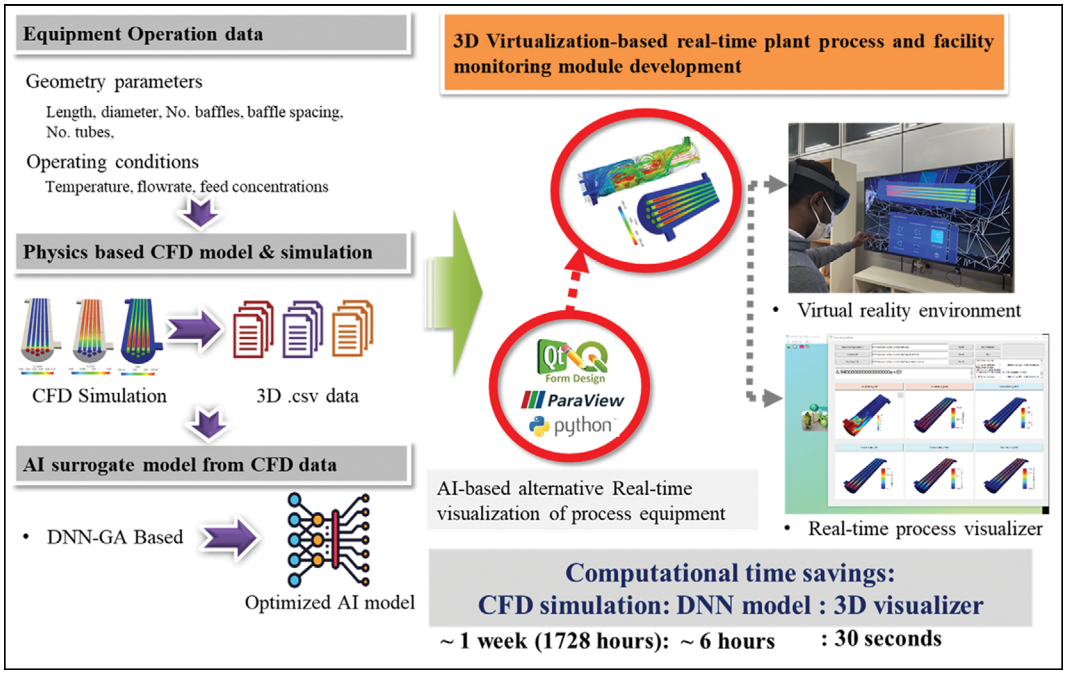

Fig. 10. Summary of the presented strategy with obtained results.

dering the data into 3D images of png and glTF formats. A graphic user interface and a virtual reality environment were created to visualize these results. The GUI gave a real-time monitoring experience as the process output changes with respect to the changing input condition. This implemented solution provides a new direction for designing and deploying digital twins. The method is also useful for online optimization of process variables and efficient manipulation of control variables.

ACKNOWLEDGEMENT

This research was supported by INHA UNIVERSITY Research Grant.

REFERENCES

1. A. Fuller, Z. Fan, C. Day and C. Barlow, *IEEE Access*, **8**, 108952 (2020).
2. R. Vrabič, J. A. Erkoyuncu, P. Butala and R. Roy, *Procedia Manuf.*, **16**, 139 (2018).
3. X. Fei, N. Shah, N. Verba, K. M. Chao, V. Sanchez-Anguix, J. Lewandowski, A. James and Z. Usman, *Future Generation Comput Syst.*, **90**, 435 (2019).
4. Q. Qi and F. Tao, *IEEE Access*, **6**, 3585 (2018).
5. C. Mandolla, A. M. Petruzzelli, G. Percoco and A. Urbinati, *Comput. Ind.*, **109**, 134 (2019).
6. S. Rokka Chhetri, S. Faezi, A. Canedo and M. Abdullah Al Faruque, Proceedings of the International Conference on Internet of Things Design and Implementation (2019).
7. Y. He, J. Guo and X. Zheng, *IEEE Signal Process. Mag.*, **35**, 120 (2018).
8. X. Chen, E. Kang, S. Shiraishi, V. M. Preciado and Z. Jiang, Proceedings - 21st ACM/IEEE International Conference on Model Driven Engineering Languages and Systems, MODELS 2018 144 (2018).
9. R. Magargle, L. Johnson, P. Mandloi, P. Davoudabadi, O. Kesarkar, S. Krishnaswamy, J. Batteh and A. Pitchaikani, *Proceedings of the 12th International Modelica Conference*, Prague, Czech Republic, May 15-17, 2017 **132**, 35 (2017).
10. A. M. Karadeniz, İ. Arif, A. Kanak and S. Ergün, *Proceedings - IEEE International Symposium on Circuits and Systems*, **2019-May** (2019).
11. A. Coraddu, L. Oneto, F. Baldi, F. Cipollini, M. Atlar and S. Savio, *Ocean Eng.*, **186**, 106063 (2019).
12. A. M. Madni, C. C. Madni and S. D. Lucero, *Systems*, **7**, 7 (2019).
13. A. Bilberg and A. A. Malik, *CIRP Annals*, **68**, 499 (2019).
14. E. H. Glaessgen and D. S. Stargel, Collection of Technical Papers - AIAA/ASME/ASCE/AHS/ASC Structures, Structural Dynamics and Materials Conference (2012).
15. D. Petrik and G. Herzwurm, IWSiB 2019 - *Proceedings of the 2nd ACM SIGSOFT International Workshop on Software-Intensive Business: Start-Ups, Platforms, and Ecosystems*, Co-Located with ESEC/FSE 2019 1 (2019).
16. Y. Zheng, S. Yang and H. Cheng, *J. Ambient Intelligence and Humanized Computing*, **10**, 1141 (2019).
17. D. Q. Gbadago, J. Moon, M. Kim and S. Hwang, *Chem. Eng. J.*, **409**, 128163 (2021).
18. H. Kim, M. Park, C. W. Kim and D. Shin, *Comput. Chem. Eng.*, **125**, 476 (2019).
19. J. S. Sterrett and H. G. Mcllvried, *Ind. Eng. Chem. Process Des. Dev.*, **13**, 54 (1974).